Proceedings of 20th International Congress on Acoustics, ICA 2010

23-27 August 2010, Sydney, Australia

Multibubble cavitation inception: Effects of bubble-bubble interaction under negative pressure

Masato Ida

J-PARC Center, Japan Atomic Energy Agency, 2-4 Shirakata-Shirane, Tokai-mura, Naka-Gun, Ibaraki 319-1195, Japan

PACS: 47.55.dp; 47.55.dd

ABSTRACT

Multibubble effects on cavitation inception are studied in detail to show that bubble-bubble interaction can change the inception process of cavitation in a variety of ways. In an effort to develop a high-power pulsed neutron source which uses a giant proton accelerator and liquid mercury, we have attempted to use microbubbles to reduce cavitation damage of the mercury vessels caused by proton-induced intense pressure waves. From an off-line experiment, we found that cavitation of liquid mercury is suppressed by injecting a sufficient amount of gas microbubbles into mercury. This observation was the starting point of our multibubble study on cavitation inception. Using a simple multibubble model in which Rayleigh–Plesset type equations are coupled through the bubble-emitted pressure waves, we first showed that microbubbles can in certain cases suppress explosive growth of cavitation bubbles under negative pressure, implying a significant effect of injected microbubbles on cavitation inception. We then performed a more detailed numerical study on cavitation in multibubble cases and found that several different patterns of bubble dynamics, such as competitive growth and interrupted expansion, are possible in the early stage of cavitation. From this detailed study we also found that the instantaneous unstable equilibrium radii of growing bubbles play an essential role in these processes. These findings unveil the complex nature of interacting bubbles under negative pressure.

INTRODUCTION

The J-PARC (Japan Proton Accelerator Research Complex) project [1] is a R&D project on the development and use of a MW-class proton accelerator promoted by The Japan Atomic Energy Agency and the High Energy Accelerator Research Organization. One of the aims of this project is to provide a high-power spallation neutron source to be used in materials and life sciences. In the neutron source being developed, liquid mercury flowing inside a metal target vessel is bombarded by high-intensity proton beams to produce high neutron fluxes. The accelerated proton beams have a maximum energy of 3 GeV and are repeatedly injected into the mercury at a repetition rate of 25 Hz.

In the development of the neutron source, cavitation in liquid mercury and the resulting damage are now significant problems. From several different experiments [2–6], it was suggested that high-intensity pressure waves produced in liquid mercury by the enormous energy of proton beams cause cavitation of mercury and it will significantly reduce the lifetime of the target vessel by causing cavitation damage. Given these findings, we and collaborators are now performing various investigations to overcome this critical issue [7–13]. Our present aim is to propose a technique to reduce the cavitation damage or suppress the cavitation itself.

One of the promising techniques to reduce cavitation damage is *microbubble injection*. From several numerical studies [8, 12], it was suggested that microbubbles in mercury can significantly decrease the amplitude of pressure waves and may reduce cavitation damage. Recently, this numerical prediction was confirmed experimentally from a water study [13]. Recent studies also suggested that microbubbles can suppress cavitation inception. In Refs. [7, 11], we showed numerically and theoretically that the pressure waves emitted by injected microbubbles decrease the amplitude of negative pressure in liquid, which is the trigger of cavitation, and hence cavitation inception is suppressed if the size and number density of bubbles are appropriate. In Ref. [9], we confirmed experimentally the validity of this theoretical prediction.

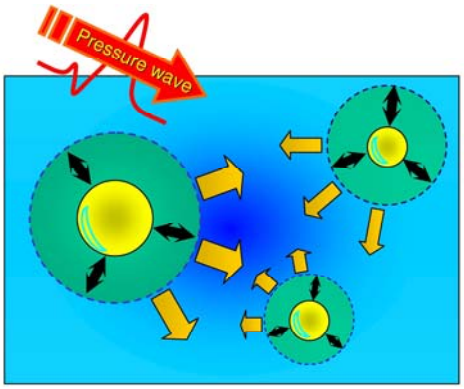

Fig. 1. Bubble-bubble interaction through pressure waves. When the pressure of a liquid is changed by a propagating pressure wave, bubbles immersed in the liquid begin volume oscillation and emit pressure waves. Bubble-bubble interaction through the bubble-emitted pressure waves leads to a variety of phenomena.

To more deeply understand the mechanism of cavitation suppression by microbubbles, and also to gain a deeper insight

into the inception process of cavitation, we perform a detailed numerical study on cavitation inception [14]. As in our previous study, we focus our attention on acoustic interaction of bubbles. The coupling of bubbles through pressure waves, a kind of bubble-bubble interaction (Fig. 1), is known to lead to a variety of phenomena that single bubbles can never exhibit, such as attraction and repulsion of pulsating bubbles [15–20], the appearance of "transition frequencies" [20, 21], avoided crossings of resonance frequencies [22], and filamentary structure formation in a strong sound field [23, 24] (see, e.g., Refs. [25–31] for more about the effects of bubble-bubble interaction). In this paper, we consider cavitation inception in a system where a number of cavitation nuclei (assumed to be gas microbubbles) exist and may interact with each other. The theoretical model used is the coupled Rayleigh–Plesset equations which describe the radial motion of bubbles interacting through pressure waves. The liquid is assumed to be water, a liquid much more familiar than mercury. Taking bubble-bubble interaction into account, we examine in detail the dynamics of cavitation nuclei under negative pressure. First we show that the suppression of cavitation inception reported in Ref. [7] can occur in water as well if the size and inter-bubble distance are properly set. Then, we examine several details of the numerical result. Particular attention is focused on the effective cavitation pressure (dynamic Blake threshold) of the interacting bubbles and the transition region in parameter space where the bubble's behaviour drastically changes as the inter-bubble distance changes. In the present investigation we found that the inception process of cavitation in multi-nuclei cases can be much more complex than in single-nuclei cases and that a variety of patterns of inception are possible.

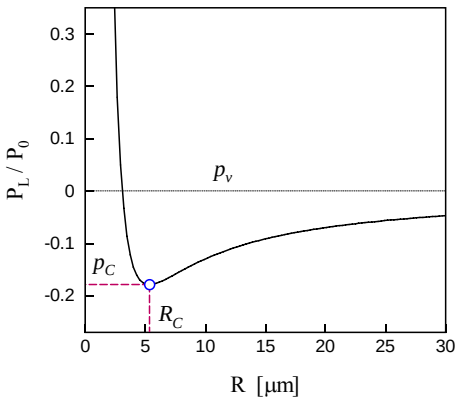

Fig. 2. $p_L - R$ curve for $R_0 = 2$ μm, $p_v = 0$ Pa, and $\kappa = 1$. The liquid pressure p_L is normalized by the atmospheric pressure P_0. p_C and R_C are the threshold pressure and critical radius, respectively.

BRIEF REVIEW OF SINGLE-BUBBLE CAVITATION

One of the well-known notions of cavitation in single-bubble cases under quasistatic conditions is the Blake threshold [32–34]. For liquid pressures below a threshold value, a gas microbubble (cavitation nucleus) does not have an equilibrium radius and thus undergoes unbounded expansion, which implies the occurrence of cavitation. The threshold liquid pressure is called the Blake threshold pressure and the bubble radius at the threshold is called the Blake critical radius. These critical values are obtained by solving the pressure balance equation at the bubble surface,

$$p_L = p_b - \frac{2\sigma}{R}, \tag{1}$$

where p_L is the liquid pressure, p_b is the internal pressure of the bubble given by

$$p_b = \left(P_0 + \frac{2\sigma}{R_0} - p_v\right)\left(\frac{R_0}{R}\right)^{3\kappa} + p_v, \tag{2}$$

σ is the surface tension, R is the bubble radius at p_L, $P_0 = 0.1013$ MPa is the atmospheric pressure, R_0 the ambient radius of the bubble, p_v the vapour pressure, and κ the polytropic exponent of the gas inside the bubble. Equation (1) describes the balance between p_L and p_b through the surface tension force $2\sigma/R$. An example of the $p_L - R$ curve given by Eq. (1) with $R_0 = 2$ μm is shown in Fig. 2. Here, we neglected the vapour pressure for simplicity and $\kappa = 1$, that is, the bubble interior is isothermal. This result reveals that for p_L below a threshold value p_C, no bubble radius exists that satisfies Eq. (1). The threshold pressure is

$$p_C = p_v - \sqrt{\frac{32\sigma^3}{27\left(P_0 + \frac{2\sigma}{R_0} - p_v\right)R_0^3}}, \tag{3}$$

and the corresponding critical radius is

$$R_C = \sqrt{\frac{3}{2\sigma}\left(P_0 + \frac{2\sigma}{R_0} - p_v\right)R_0^3}. \tag{4}$$

For $p_C < p_L < p_v$, Eq. (1) has two roots corresponding to equilibrium radii [32–36]. The smaller root represents the stable equilibrium radius, at which the bubble can be stationary. On the other hand, the larger root represents the unstable equilibrium radius, where a small deviation in bubble radius results in rapid shrink or explosive expansion. As shown below, the unstable equilibrium radius plays an important role in our study.

In dynamic cases where the liquid pressure varies rapidly, the above scenario is only a rough description. Detailed theoretical and numerical investigations of single-bubble cavitation have revealed several dynamic effects. Researchers have found, for example, that even if $\min[p_L(t)] > p_C$, the instantaneous bubble radius can in certain conditions be greater than the unstable equilibrium radius in the transient period, resulting in the inception of cavitation [33–38]. This observation says that the effective threshold pressure can be different from that in the quasistatic case.

As briefly reviewed above, a number of useful insights into single-bubble cavitation have been published. In reality, however, not only one but many cavitation nuclei exist and may interact with each other. Single-bubble study is thus not sufficient to fully understand cavitation in practical situations. As shown in the following sections, bubble-bubble interaction can drastically change the inception processes of cavitation in several ways.

MODEL EQUATIONS AND SETTINGS

We assume the cavitation nuclei to be spherical gas microbubbles. The theoretical model used to describe their evolution is the coupled Rayleigh–Plesset equations, which read

$$R_i\ddot{R}_i + \frac{3}{2}\dot{R}_i^2 = \frac{1}{\rho}p_{s,i} - \sum_{j=1,j\neq i}^{N}\frac{1}{D_{ij}}\frac{d(R_j^2\dot{R}_j)}{dt}, \quad (5)$$

$$p_{s,i} = p_{b,i} - \frac{2\sigma}{R_i} - \frac{4\mu\dot{R}_i}{R_i} - p_L(t), \quad (6)$$

$$i = 1, 2, \cdots, N ,$$

where $R_i = R_i(t)$ is the time-dependent radius of bubble i, D_{ij} is the distance between the centres of bubbles i and j, $p_L(t)$ is the liquid pressure in the far field, N is the number of bubbles, and the overdots denote the time derivative d/dt. The surrounding liquid is assumed to be water of density $\rho = 1000$ kg/m^3, viscosity $\mu = 1.002\times10^{-3}$ Pa s, and surface tension $\sigma = 0.0728$ N/m. Liquid compressibility is neglected since we are not interested in the details of bubble collapse. The bubble content is assumed to be an ideal gas, and the internal pressure of bubble i ($p_{b,i}$) is thus given by

$$p_{b,i} = \left(P_0 + \frac{2\sigma}{R_{i0}}\right)\left(\frac{R_{i0}}{R_i}\right)^{3\kappa_i}, \quad (7)$$

where R_{i0} and κ_i are the ambient radius and polytropic exponent, respectively, of bubble i. The vapour pressure and mass exchange across the bubble surface are neglected. Assuming that the bubble content is isothermal, κ_i is set to unity. Since translation of bubbles and high-order terms depending on the translational velocity [18, 39, 40] are neglected in this model, we set the inter-bubble distances D_{ij} to be much greater than $R_{i0} + R_{j0}$.

This nonlinear system of equations describes the radial motion of N spherical bubbles coupled through the bubble-emitted pressure waves. In this system, the bubbles' radial motion is driven by both the liquid pressure and the pressures from the neighbouring bubbles described by the last term of Eq. (5). This term was derived by a formula for the pressure wave emitted by a pulsating sphere [7, 17]

$$p_j = \frac{\rho}{r_j}\frac{d(R_j^2\dot{R}_j)}{dt} + O\left(\frac{1}{r_j^4}\right), \quad (8)$$

where r_j is the distance measured from the centre of bubble j.

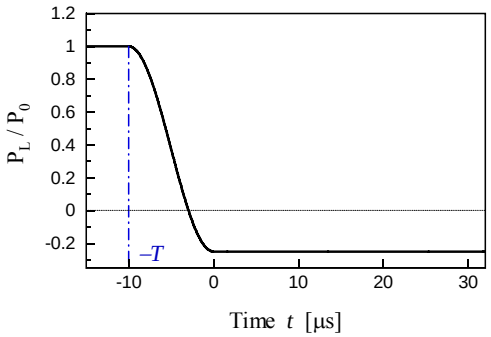

Fig. 3. Pressure-time history assumed in the present study. The shown history is for $T = 10$ μs. A similar pressure profile observed experimentally can be found in, e.g., Ref. [6].

The time history of the far-field liquid pressure is assumed as

$$p_L(t) = \begin{cases} P_0 & \text{for } t < -T, \\ P_0 + W(P_{ng} - P_0) & \text{for } -T \le t \le 0, \\ P_{ng} & \text{otherwise,} \end{cases} \quad (9)$$

with

$$W = \frac{1 - \cos\left[\frac{\pi}{T}(t+T)\right]}{2}, \quad (10)$$

where P_{ng} is a constant negative value and T is the period of the decompression process from P_0 to P_{ng}. This function represents a constant negative pressure following a sinusoidal decompression and is continuous up to the first time derivative (see Fig. 3). In the following discussions, P_{ng} and T are used as control parameters. When one sets $T \to 0$, Eq. (9) is reduced to a step change like that considered in Refs. [35, 36, 38, 41]. The initial conditions are

$$R_i(t = -T) = R_{i0}, \quad (11)$$

$$\dot{R}_i(t = -T) = 0, \quad (12)$$

that is, the bubbles are initially at equilibrium.

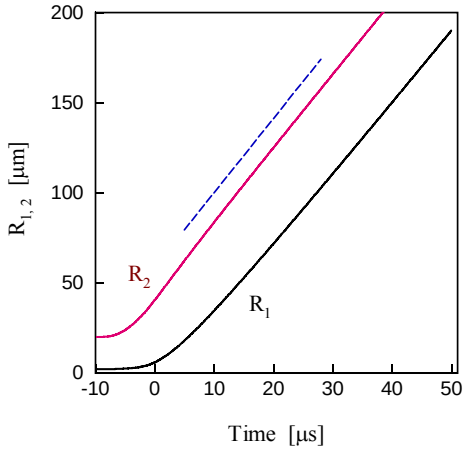

Fig. 4. Radius-time curves in single-bubble cases (for $D_{12} \to \infty$). The ambient radii of the bubbles are $R_{10} = 2$ μm and $R_{20} = 20$ μm. The dashed line denotes the slope determined by Eq. (13).

NUMERICAL INVESTIGATIONS

Competitive growth of interacting bubbles

Let us consider the dynamics of two non-identical bubbles (bubbles 1 and 2) under negative pressure. An example of a single-bubble case (i.e., for $D_{12} \to \infty$) is shown in Fig. 4. Here we set $R_{10} = 2$ μm, $R_{20} = 20$ μm, $\kappa_{1,2} = 1$, $P_{ng} = -0.25P_0$, and $T = 10$ μs, and the corresponding threshold pressures are $p_{C1} = -0.179P_0$ for bubble 1 and $p_{C2} = -0.007P_0$ for bubble 2. Since P_{ng} well exceeds the threshold pressures, both bubbles undergo explosive expansion. The response of bubble 2 in the decompression process is faster than that of bubble 1, because bubble 2 has a much

higher threshold pressure than that of bubble 1. Hence, the explosive expansion of bubble 2 begins earlier than that of bubble 1. After the transient motion has decayed, the expansion rates of both bubbles converge to an almost constant value determined by

$$\frac{dR}{dt} \approx \sqrt{\frac{2(p_v - p_L)}{3\rho}}. \qquad (13)$$

These observations are consistent with the well-known behaviour of single cavitation bubbles. As mentioned above, the threshold pressure in dynamic cases is in general different from the value given by the quasistatic theory. The threshold pressure of bubble 1 in the present case ($T = 10$ μs) is slightly higher (only about 1.7% [14]) than the theoretical prediction. The dynamic threshold comes closer to the quasistatic prediction as T increases.

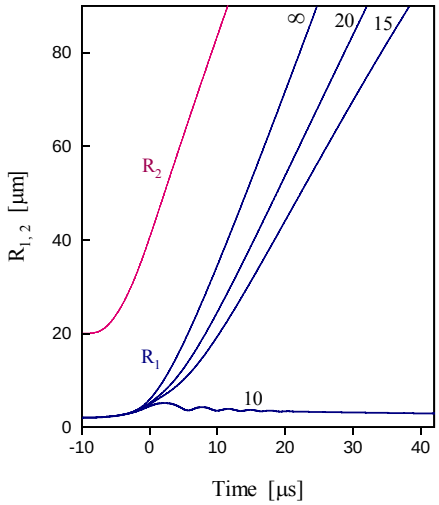

Fig. 5. Radius-time curves for $P_{ng} = -0.25P_0$ and four different D_{12} values. The numbers denote $D_{12}/(R_{10} + R_{20})$. The curves of R_2 for different D_{12} values are indistinguishable. For $D_{12} = 10(R_{10} + R_{20})$, bubble 1 cannot grow significantly although p_L is well below the threshold pressure of the bubble.

For finite D_{12}, the dynamics of the bubbles can have a different pattern. In Fig. 5 we show the results for $P_{ng} = -0.25P_0$ with four different values of D_{12}. From the figure, one finds that the expansion rate of bubble 1 is decreased as D_{12} decreases, and the explosive expansion of this bubble is finally suppressed for $D_{12} = 10(R_{10} + R_{20})$, although the negative pressure considered here clearly exceeds its threshold pressure: the expansion ratio of bubble 1, $\max[R_1(t)]/R_{10}$, in this case is only about 2.57. No considerable change occurs in the dynamics of bubble 2 in the shown period, because bubble 1 is too small to cause it. The results presented here prove that the suppression phenomenon reported in Refs. [7, 11] is not inherent in liquid mercury and can also occur in water, whose material properties are greatly different from those of mercury. In what follows, we discuss details of this phenomenon.

The above numerical result suggests that the *effective* threshold pressure of bubble 1 in the case of $D_{12} = 10(R_{10} + R_{20})$ is much lower than that predicted by the quasistatic theory (3) and a more intense negative pressure is thus needed to cavitate bubble 1. Figure 6 shows the dynamics of bubble 1 for $D_{12} = 10(R_{10} + R_{20})$ and four different values of P_{ng}. From this, the effective threshold pressure of bubble 1 is deduced to be within the range of $-0.270P_0 \sim -0.276P_0$, the absolute value of which is 1.5 times greater than the theoretical prediction.

This significant change in threshold pressure is due to the positive pressure wave emitted by bubble 2. Bubbles expanding explosively under negative pressure emit positive pressure waves through their radial motion [7, 11]. The positive pressure waves reduce the magnitude of the negative pressure in the surrounding liquid, leading to the need for a more intense negative (far-field) pressure to cavitate. The positive pressure from bubble 2 is estimated by the following simple formula [7]:

$$p_2(t) = -\frac{4R_2(t)}{3D_{12}} P_{ng}, \qquad (14)$$

which is given using Eqs. (8) and (13) under the assumption of $\ddot{R}_2 \approx 0$. Since P_{ng} is negative, $p_2(t)$ is positive. The total pressure acting on bubble 1 is thus

$$P_{ng} + p_2 = \left(1 - \frac{4R_2(t)}{3D_{12}}\right) P_{ng}, \qquad (15)$$

which is clearly higher than the far-field liquid pressure.

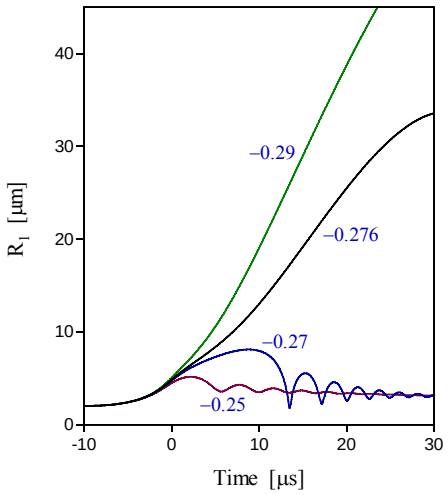

Fig. 6. Radius-time curves of bubble 1 for $D_{12} = 10(R_{10} + R_{20})$ and four different P_{ng} values selected around the effective threshold pressure of the bubble. The numbers in the panel denote P_{ng}/P_0.

The observed suppression of explosive expansion, or competitive growth of bubbles, occurs also for other couples of bubbles. In Fig. 7 we show the expansion ratios of bubbles, $\max[R_j(t)]/R_{j0}$, for $R_{10} = 2$ μm, $P_{ng} = -0.25P_0$, and $t \le 20$ μs as functions of R_{20}. Here the inter-bubble distance was fixed as $D_{12} = 220$ μm, which corresponds to $10(R_{10} + R_{20})$ in the previous example. From this figure one finds that the explosive expansion of bubble 1 is completely suppressed when $R_{20} \ge 17$ μm. This figure also suggests that when $R_{20} < R_{10}$ the expansion of bubble 2 can be suppressed by bubble 1, and that for $R_{20} > R_{10}$ the expansion ratio of bubble 2 decreases monotonically as R_{20} increases. The latter is due to the fact that the expansion rate of bubble 2 has an almost constant value determined by Eq. (13) although R_{20} changes, and hence a larger R_{20} gives a smaller expansion ratio. The above results prove that the suppression of explosive expan-

sion can occur if the bubbles' ambient radii and inter-bubble distance are appropriately set.

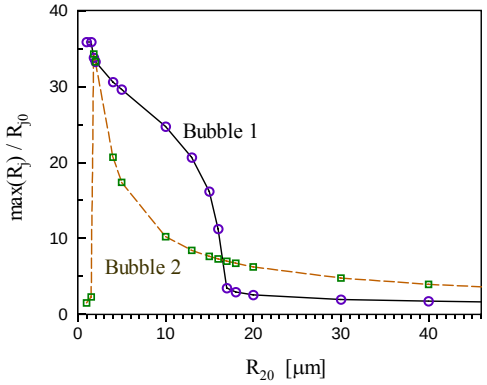

Fig. 7. Expansion ratios of the bubbles as functions of R_{20}. Shown are for $R_{10} = 2$ μm, $P_{ng} = -0.25P_0$, and $t \le 20$ μs.

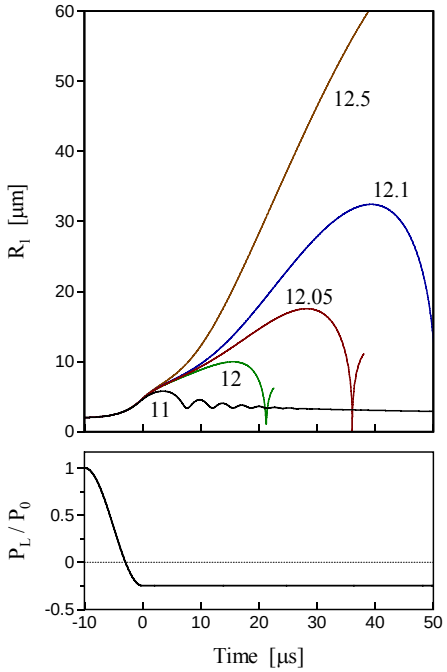

Fig. 8. Radius-time curves of bubble 1 for $P_{ng} = -0.25P_0$ and five different D_{12}. The numbers denote $D_{12}/(R_{10} + R_{20})$. For $D_{12} = 12(R_{10} + R_{20}) \sim 12.1(R_{10} + R_{20})$, the bubble collapses although p_L (the lower panel) holds constant at a negative value.

Interrupted expansion of an interacting bubble

Figure 5 implies that a transition of bubble dynamics takes place in a parameter range between $D_{12} = 10(R_{10} + R_{20})$ and $15(R_{10} + R_{20})$. Here we clarify what occurs in the transition region. In Fig. 8, we show the radius-time curves of bubble 1 for $R_{10} = 2$ μm, $R_{20} = 20$ μm, $P_{ng} = -0.25P_0$, and five different D_{12} values selected from the above-mentioned parameter range. The other parameters were set as in the above examples. As shown previously, decreasing D_{12} results in the decrease of the expansion rate of bubble 1. In the parameter range considered here, however, one more interacting change can be found: The expansion of bubble 1 is interrupted at a moment. In the results for $D_{12} = 12(R_{10} + R_{20}) \sim 12.1(R_{10} + R_{20})$, one finds that bubble 1 first expands considerably, but then turns into collapse although p_L holds constant at a negative value that exceeds the quasistatic threshold pressure. Such behaviour is not allowed for isolated bubbles. This observation suggests that bubble-bubble interaction sometimes causes a significant change in the lifetime of cavitating bubbles.

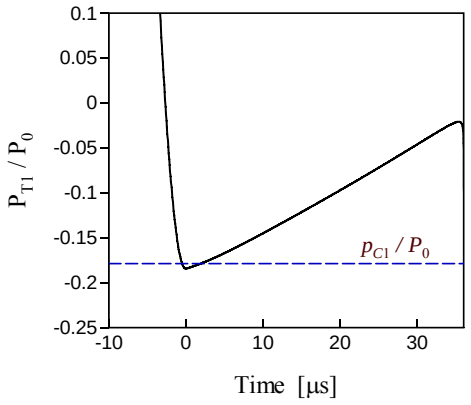

Fig. 9. Total driving pressure on bubble 1 for $D_{12} = 12.05(R_{10} + R_{20})$. The dashed line denotes the quasistatic threshold pressure of bubble 1 ($p_{C1} = -0.179P_0$).

Let us consider the mechanism underlying this observation. As known from Eq. (14), the total pressure acting on bubble 1 increases as time goes on [i.e., as $R_2(t)$ becomes greater]. Indeed, the total pressure at bubble 1's position determined numerically by

$$p_{T1} = p_L + \frac{\rho}{D_{12}} \frac{d(R_2^2 \dot{R}_2)}{dt} \qquad (16)$$

increases for $t > 0$ (see Fig. 9). From this, one may presume that the interruption of bubble expansion occurs when the total pressure rises above the quasistatic threshold pressure of bubble 1. This conjecture is, however, incorrect. In most periods, the total pressure is clearly higher than the threshold pressure except for a short duration around $t = 0$, and their crossing points are far from the time of interruption (Fig. 9). The notion of threshold pressure is therefore useless for the present purpose.

To correctly understand the numerical observation, we suggest using the unstable equilibrium radius. As mentioned in the previous section, a bubble has an unstable equilibrium radius under the condition of $p_C < p_L < p_v$. We reveal here that the unstable equilibrium radius plays an essential role in the occurrence of interrupted expansion. Figure 10 shows the radius-time curves of bubble 1 for three different D_{12} values and the corresponding unstable equilibrium radius (called hereafter R_{Ue1}). Here R_{Ue1} was determined using Eq. (1) by replacing p_L with p_{T1} (16). Since p_{T1} is time dependent, R_{Ue1} in the present case varies in time. For $D_{12} = 12.5(R_{10} + R_{20})$, R_1 well exceeds R_{Ue1} for $0\,\mu s < t < 37\,\mu s$, and hence bubble 1 can expand rapidly as a single bubble does. For $D_{12} = 12.05(R_{10} + R_{20})$, R_1 is slightly larger than R_{Ue1} for $0\,\mu s < t < 22\,\mu s$ and bubble 1 expands mildly during this period. However, R_1 is exceeded by R_{Ue1} at about $t = 22\,\mu s$, and then bubble 1 stops expanding and

begins collapsing. For $D_{12} = 12(R_{10} + R_{20})$, R_1 is smaller than or almost equal to R_{Ue1} in most periods. Hence, bubble 1 cannot expand considerably and behaves as a stable bubble under positive absolute pressure. As can be seen in Fig. 10(b), the crossing point of R_1 with R_{Ue1} correlates well with the time for bubble 1 to stop accelerating. This observation proves that the instantaneous unstable equilibrium radius can be used as a probe for the interruption of bubble expansion. As we showed in Ref. [14], qualitatively the same results are obtained even for smaller T.

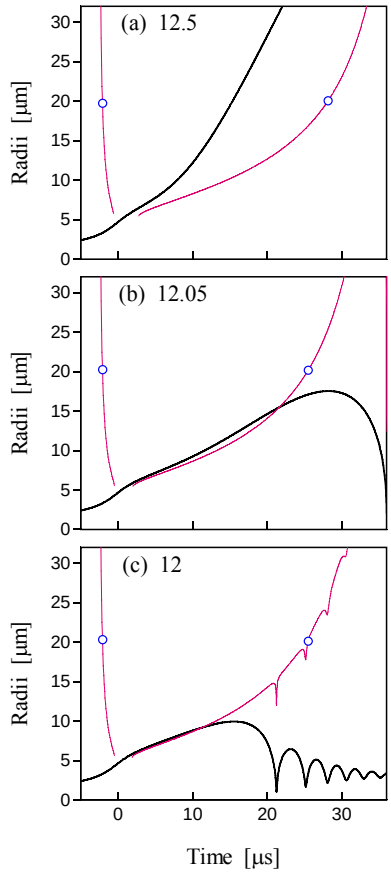

Fig. 10. Radius and unstable equilibrium radius of bubble 1 for different D_{12} values as functions of time. The thick curves denote R_1 and the thin curves with circles denote R_{Ue1}. The numbers denote $D_{12}/(R_{10} + R_{20})$.

CONCLUDING REMARKS

We have studied the inception processes of cavitation in multibubble cases, where multiple cavitation nuclei exist and interact with each other. We have shown that bubble-bubble interaction changes the dynamics of cavitation bubbles in a variety of ways. Performing numerical simulations of the dynamics of non-identical bubbles under negative pressure, we have demonstrated that the suppression of the explosive expansion of small bubbles by bubbles expanding earlier, recently found for liquid mercury [7, 11], is possible in water as well. To deeply understand the numerical observation, we have discussed the effective threshold pressure of interacting bubbles. We found that even a bubble can significantly decrease (by about 50%) the effective threshold pressure of a smaller neighboring bubble. This change of threshold value is much more significant than that caused by the dynamic effect due to rapid change in the far-field liquid pressure.

From a detailed analysis of the transition region where the dynamics of the suppressed bubble drastically changes as the inter-bubble distance changes, we have revealed that the explosive expansion of a bubble under negative pressure can be interrupted and turn into collapse even though the far-field liquid pressure remains well below the bubble's (quasistatic) threshold pressure. Using the notion of unstable equilibrium radius, we have found that the interruption of bubble expansion takes place when the instantaneous bubble radius is exceeded by the instantaneous unstable equilibrium radius determined using the total pressure acting on the bubble. Both the suppression and interruption of bubble expansion are caused by the pressure wave that a neighboring bubble emits when it grows.

These findings provide a new insight into the inception process of cavitation and the effect of bubble-bubble interaction, and could be a key to understanding the complex behavior of cavitation bubbles in practical situations where a large number of cavitation nuclei exist and interact with each other. The present findings would also be useful in deeply understanding bubble dynamics under negative pressure found, e.g., in experiments of single-bubble or multibubble sonoluminescence.

ACKNOWLEDGEMENTS

This work was partly supported by the Ministry of Education, Culture, Sports, Science, and Technology of Japan (MEXT) through a Grant-in-Aid for Young Scientists (B) (No. 20760122).

REFERENCES

[1] S. Nagamiya, J. Nucl. Mater. 343, 1 (2005); Y. Ikeda, J. Nucl. Mater. 343, 7 (2005); S. Nagamiya, Nucl. Phys. A 774, 895 (2006).
[2] M. Futakawa, H. Kogawa, and R. Hino, J. Phys. IV 10, 237 (2000).
[3] B. W. Riemer, J. R. Haines, J. D. Hunn, D. C. Lousteau, T. J. McManamy, and C.C. Tsai, J. Nucl. Mater. 318, 92 (2003); J. D. Hunn, B. W. Riemer, and C.C. Tsai, J. Nucl. Mater. 318, 102 (2003).
[4] M. Futakawa, T. Naoe, H. Kogawa, C.-C. Tsai, and Y. Ikeda, J. Nucl. Sci. Technol. 40, 895 (2003).
[5] M. Futakawa, T. Naoe, H. Kogawa, M. Teshigawara, and Y. Ikeda, J. Nucl. Mater. 356, 168 (2006).
[6] M. Ida, T. Naoe, and M. Futakawa, Phys. Rev. E 75, 046304 (2007).
[7] M. Ida, T. Naoe, and M. Futakawa, Phys. Rev. E 76, 046309 (2007).
[8] K. Okita, S. Takagi, and Y. Matsumoto, J. Fluid Sci. Tech. 3, 116 (2008).
[9] T. Naoe, M. Ida, and M. Futakawa, Nucl. Instr. and Meth. A 586, 382 (2008).
[10] B. Riemer, J. Haines, M. Wendel, G. Bauer, M. Futakawa, S. Hasegawa, and H. Kogawa, J. Nucl. Mater. 377, 162 (2008).
[11] M. Ida, T. Naoe, and M. Futakawa, Nucl. Instr. Meth. Phys. Res. A 600, 367 (2009).
[12] T. Lu, R. Samulyak, and J. Glimm, J. Fluids Eng. 129 (2007) 595.
[13] T. Naoe, H. Kogawa, M. Futakawa, and M. Ida, unpublished.
[14] M. Ida, Phys. Fluids 21, 113302 (2009).
[15] L. A. Crum, J. Acoust. Soc. Am. 57, 1363 (1975).
[16] E. A. Zabolotskaya, Sov. Phys. Acoust. 30, 365 (1984).
[17] R. Mettin, I. Akhatov, U. Parlitz, C. D. Ohl, and W. Lauterborn, Phys. Rev. E 56, 2924 (1997).
[18] A. A. Doinikov, Phys. Rev. E 64, 026301 (2001).
[19] M. Ida, Phys. Rev. E 67, 056617 (2003).
[20] M. Ida, Phys. Fluids 17, 097107 (2005).
[21] M. Ida, Phys. Lett. A 297, 210 (2002); M. Ida, J. Phys. Soc. Japan 71, 1214 (2002).

[22] M. Ida, Phys. Rev. E 72, 036306 (2005).
[23] U. Parlitz, C. Scheffczyk, I. Akhatov, and W. Lauterborn, Chaos, Solitons & Fractals 5, 1881 (1995).
[24] I. Akhatov, U. Parlitz, and W. Lauterborn, Phys. Rev. E 54, 4990 (1996).
[25] A. Shima, ASME J. Basic Eng. 93, 426 (1971).
[26] R. H. Smith and R. B. Mesler, ASME J. Basic Eng. 94, 933 (1972).
[27] G. L. Chahine and H. L. Liu, J. Fluid Mech. 156, 257 (1985).
[28] S. Fujikawa and H. Takahira, Acustica 61, 188 (1986).
[29] A. Harkin, T. J. Kaper, and A. Nadim, J. Fluid Mech. 445, 377 (2001).
[30] M. Ida, Phys. Rev. E 79, 016307 (2009).
[31] R. Manasseh and A. Ooi, Bubble Science, Engineering and Technology 1 (2009) 58 and references therein.
[32] C. E. Brennen, *Cavitation and Bubble Dynamics* (Oxford University Press, New York, 1995).
[33] A. Harkin, A. Nadim, and T. J. Kaper, Phys. Fluids 11, 274 (1999).
[34] Z. C. Feng and L. G. Leal, Annu. Rev. Fluid. Mech. 29, 201 (1997).
[35] J. T. S. Ma and P. K. C. Wang, IBM J. Res. Dev. 6, 472 (1962).
[36] H.-C. Chang and L.-H. Chen, Phys. Fluids 29, 3530 (1986).
[37] A. J. Szeri and L. G. Leal, Phys. Fluids A 3, 551 (1991).
[38] C. Dugué, D. H. Fruman, J-Y. Billard, and P. Cerrutti, ASME J. Fluids Eng. 114, 250 (1992).
[39] H. N. Oguz and A. Prosperetti, J. Fluid Mech. 218, 143 (1990).
[40] H. Takahira, T. Akamatsu, and S. Fujikawa, JSME Int. J. Ser. B 37B, 297 (1994).
[41] Y. Matsumoto and A. E. Beylich, J. Fluids Eng. 107, 281 (1985).